SAWE Paper No. 3670
Category No. 18
Category No. 34

SOIL MOISTURE ACTIVE PASSIVE MISSION MASS PROPERTIES OPTIMIZATION AND ANALYSIS

Morgan L. Hendry IV and Eric M. Slimko
Jet Propulsion Laboratory, California Institute of Technology

For Presentation at the
75th SAWE International Conference
on Mass Properties Engineering
May 21-26, 2016

Denver, Colorado, USA

Permission to publish this paper in full or in part, with credit to the author and the Society, may be obtained by request to:

Society of Allied Weight Engineers, Inc.
P.O. Box 60024, Terminal Annex
Los Angeles, CA 90060

The Society is not responsible for statements or opinions in papers or discussions at the meeting.
This paper meets all regulations for public information disclosure under ITAR and EAR.

Soil Moisture Active Passive Mission Mass Properties Optimization and Analysis

Morgan L. Hendry IV[1] and Eric M. Slimko[2]
Jet Propulsion Laboratory, California Institute of Technology, Pasadena, California, 91109

ABSTRACT The Soil Moisture Active Passive (SMAP) mission creates global soil moisture measurements every 2-3 days by spinning a lightweight, ~6 meter diameter deployable mesh reflector. This represents the largest spinning antenna ever to be used on a NASA satellite. The paper discusses the mass properties challenges that were overcome in implementing the mission, including the definition of a combined imbalance term called the Effective Product of Inertia, the selection of an optimum Spun Instrument focal length and edge offset that fostered a reduced mass properties sensitivity, the inclusion of late game Spun Instrument configuration flexibility, the use of balance mass locations that leveraged the large moment arm provided by the reflector, and a subassembly measurement campaign that reduced mass properties uncertainties on testable components.

I.Introduction

THE Soil Moisture Active Passive (SMAP) satellite was designed to quantify the global water content and freeze thaw state of Earth's soil to a depth of 5 cm. This data helps inform terrestrial hydrologic models to better predict drought, flooding, regional weather patterns, crop production, and carbon fixation. SMAP fills a gap between high resolution in situ measurements and existing low resolution satellite imagery by means of an active L band synthetic aperture radar and a passive L band radiometer.

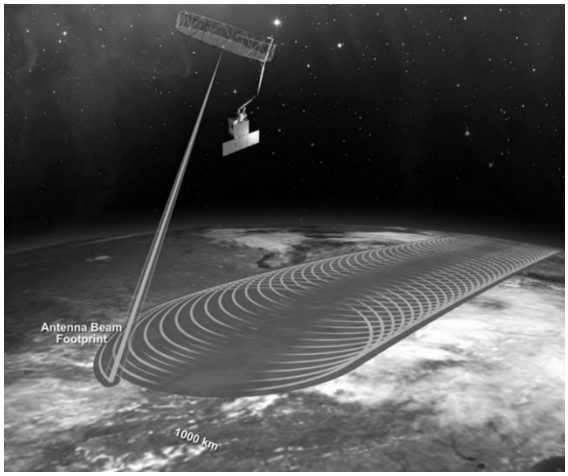

Figure 1 - SMAP satellite showing ground track generated by spinning its 6 m diameter reflector, providing high resolution ground measurements over a 1000 km swath.

[1] SMAP Mass Properties Engineer, 352M Mechanical Systems and Technology Group, 4800 Oak Grove Dr. M/S T1723-100, Pasadena, CA 91109
[2] SMAP Instrument Mechanical Systems Engineer, 3550 Payload and Small Spacecraft Mechanical Engineering, 4800 Oak Grove Dr. M/S 321-356, Pasadena, CA 91109

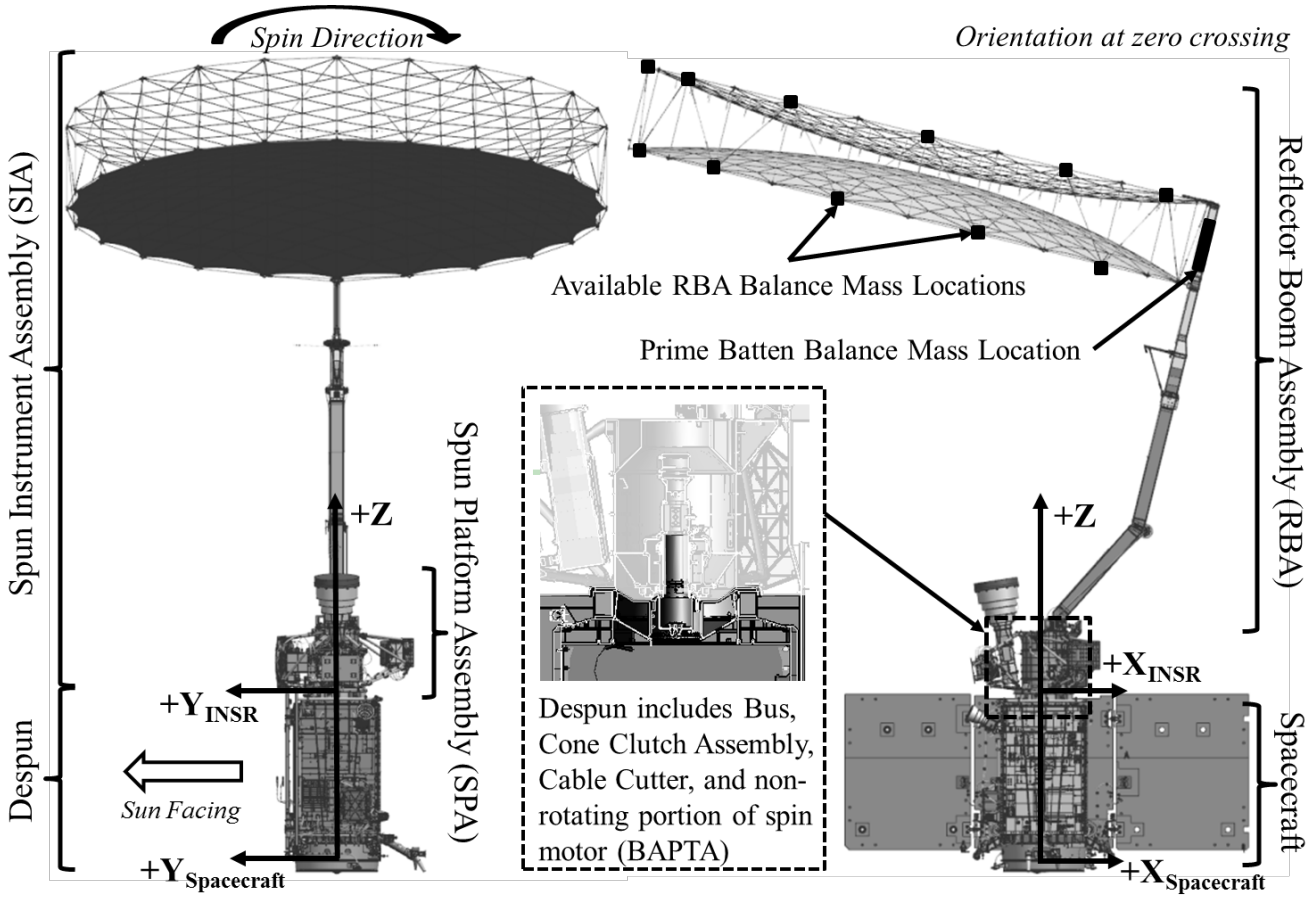

Figure 2 - SMAP Observatory and coordinate systems. Note distinction between Spacecraft and Despun. The Instrument Rotating (INSR) coordinate frame is aligned with the Spacecraft coordinate frame at zero-crossing, however it remains fixed to the Spun side geometry while spinning about the common system Z axis.

SMAP maps the Earth every 2-3 days at a resolution of 40 km from its 685 km altitude sun synchronous orbit. In order to generate a new global map within this timeframe, the SMAP instrument spins a Northrop Grumman Aerospace Systems Astro Aerospace 6 m diameter deployable mesh reflector at 14.6 RPM. This enables the satellite to project a 1000 km wide swath across the ground, as shown in Figure 1. SMAP possesses the largest spinning reflector that NASA has ever flown, and, to the project's knowledge, is the first time a deployable mesh reflector has been used in this manner.

Given the required rotation rate, certain mass properties had to be satisfied to achieve the desired ground resolution. These were bounded by a 500 mdeg nadir bias pointing error, of which 200 mdeg were allocated to mass properties imbalances. Additionally, a Spun Instrument Izz of less than 230 kg-m^2 was required to allow for robust momentum compensation in the event of a reaction wheel failure.

The reflector design and physical configuration of SMAP (Figure 2) largely prohibited spin testing of the Instrument in a flight configuration, making direct, accurate measurement of its mass properties difficult. An extensive campaign to predict, optimize, and verify the mission mass properties enabled a successful launch and spin up in the spring of 2015. Several key efforts contributed to this result:

1. The definition of a combined imbalance term called the Effective Product of

Inertia, which enabled static and dynamic imbalances to naturally counteract each other,

2. The selection of an optimum Instrument focal length and edge offset that fostered a reduced mass properties sensitivity to design changes and potential imbalances,

3. Late game Instrument configuration flexibility that enabled moderate scale redistribution of mass to counter expected developmental changes,

4. Balance mass locations that leveraged the large moment arm provided by the reflector, and

5. A subassembly measurement campaign to reduce mass properties uncertainties on testable components, allowing for the allocation of system uncertainty to untestable elements.

II.Effective Product of Inertia

Originally, requirements were levied on the separate static and dynamic components of the Spun Instrument mass properties (Table 1). Several months into the development of SMAP, the system became difficult to control within the allocated balance mass resources. Efforts to correct these imbalances through alternate configurations fell short.

The extreme sensitivity observed in this system pushed for the definition of a new requirement that aggregated the static and dynamic imbalances to a single term called the Effective Product of Inertia (EPOI). Beginning with

$$F = M_S x_S \omega^2 \tag{1}$$

where F is the force caused by static imbalances (Figure 3), M_s is the mass of the

Values	Requirement
Izz	The mass moment of inertia of the fully deployed spun instrument about the nominal instrument spin axis shall not exceed 250 kg-m^2.
Ixz, Iyz	The fully deployed spun portion product of inertias Ixz, Iyz, about the spun portion center of mass, relative to the instrument coordinate system shall be less than 0.5 kg-m^2 at the nominal operational spin rate of 14.6 RPM.
Ixy, Iyz	The fully deployed spun portion product of inertias Ixz, Iyz, about the spun portion center of mass, relative to the instrument coordinate system shall be less than 1.0 kg-m^2 during spin up from 0.0 to 14.6 RPM.
Cx, Cy	The radial distance between the spun portion of the instrument (in the deployed configuration) center of mass and the instrument spin axis shall be less than 10 mm at the nominal operational spin rate of 14.6 RPM.
Cx, Cy	The radial distance between the spun portion of the instrument (in the deployed configuration) center of mass and the instrument spin axis shall be less than 25 mm during spin up from 0.0 to 14.6 RPM.

Table 1 – Original Instrument mass properties requirements. Note separate static and dynamic allocations. It was believed early in the mission that deflection of the reflector during operation would cause significant changes to the overall Spun mass properties. This effect did not manifest itself.

Spun side, x_s is the center of mass offset of the Spun side, and ω is the spin rate, the following static and dynamic imbalance equations can be derived

$$T_{obs,static} = M_S x_S \omega^2 (z_s - z_{obs}) \tag{2}$$

$$T_{obs,dyn} = I_{s,xz} \omega^2 \tag{3}$$

Here, z_s and z_{obs} are the z center of mass (Cz) positions of the Spun Instrument and Observatory expressed in INSR coordinates, and $I_{s,xz}$ is the Spun Instrument product of inertia. Combining these terms, the net torque about the Observatory center of mass was

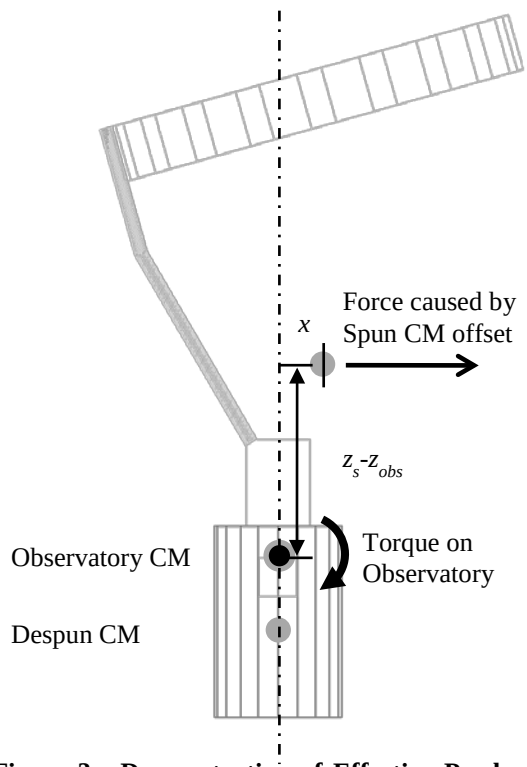

Figure 3 - Demonstration of Effective Product of Inertia (EPOI). Static and dynamic imbalances yield torques about Observatory center of mass.

$$T_{obs} = \left[I_{s,xz} + M_S x_S \left(z_s - z_{obs}\right)\right]\omega^2 \qquad (4)$$

The EPOI was defined as the bracketed term above. Broken out, and simplified to replace the Cz of the Observatory with the Cz of the Despun side, the EPOI for both the XZ and YZ planes becomes

$$I_{e,xz} = I_{s,xz} + \frac{M_s M_d}{M_s + M_d}(z_s - z_d)x_s \qquad (5)$$

$$I_{e,yz} = I_{s,yz} + \frac{M_s M_d}{M_s + M_d}(z_s - z_d)y_s \qquad (6)$$

where $I_{e,xz}$ and $I_{e,yz}$ are the Effective Ixz and Iyz Products of Inertia expressed in the INSR coordinate frame, $I_{s,xz}$ and $I_{s,yz}$ are the Spun Instrument products of inertia, M_s and M_d are the Spun and Despun masses, x_s and y_s are the x and y center of mass offset relative to the spin axis in the INSR coordinate frame, and

Value	Requirement
EPOI	The instrument shall ensure that the magnitude of the on-orbit fully deployed Spun Instrument Assembly's (SIA) X-Z (and Y-Z) effective product of inertia is less than 4.0 kg-m^2 during science operations and at the nominal antenna rotation rate with 99.8% probability.
EPOI	The instrument shall ensure that the magnitude of the on-orbit fully deployed Spun Instrument Assembly's (SIA) X-Z (and Y-Z) effective product of inertia is less than 6.0 kg-m^2 from zero to nominal antenna rotation rates with 99.8% probability.
Torque	The Instrument shall ensure that the resultant product of inertia of the spun section (IRZ) about the spin axis is less than 9.0 kg-m^2. The resultant product of inertia is the RSS of the Spun Ixz and Iyz.

Table 2 – Final Spun mass properties requirements. Note the establishment of a torque requirement to protect the BAPTA unit. Additionally, the previously defined Izz requirement was replaced with an Instrument spun momentum requirement. This allowed the spin rate of SMAP to be reduced in the event its Izz grew beyond the capability of the reaction wheels.

z_s and z_d are the Cz positions of the Spun Instrument and Despun Bus expressed in INSR coordinates.

The EPOI method worked because the Observatory cannot distinguish imbalances that are uniquely static or dynamic, only overall torques about its center of mass. As a result, dynamic imbalances were pitted against static imbalances through development, reducing the overall sensitivity of the system. This, in turn, reduced the magnitude of balance mass required to satisfy the nadir bias pointing error requirements. The only caveat to this approach was that a net torque existed between the Spun and Despun sides of the spacecraft. Here, that torque was reacted by the Boeing Bearing and Power Transfer Mechanism (BAPTA) spin motor. When new Instrument mass

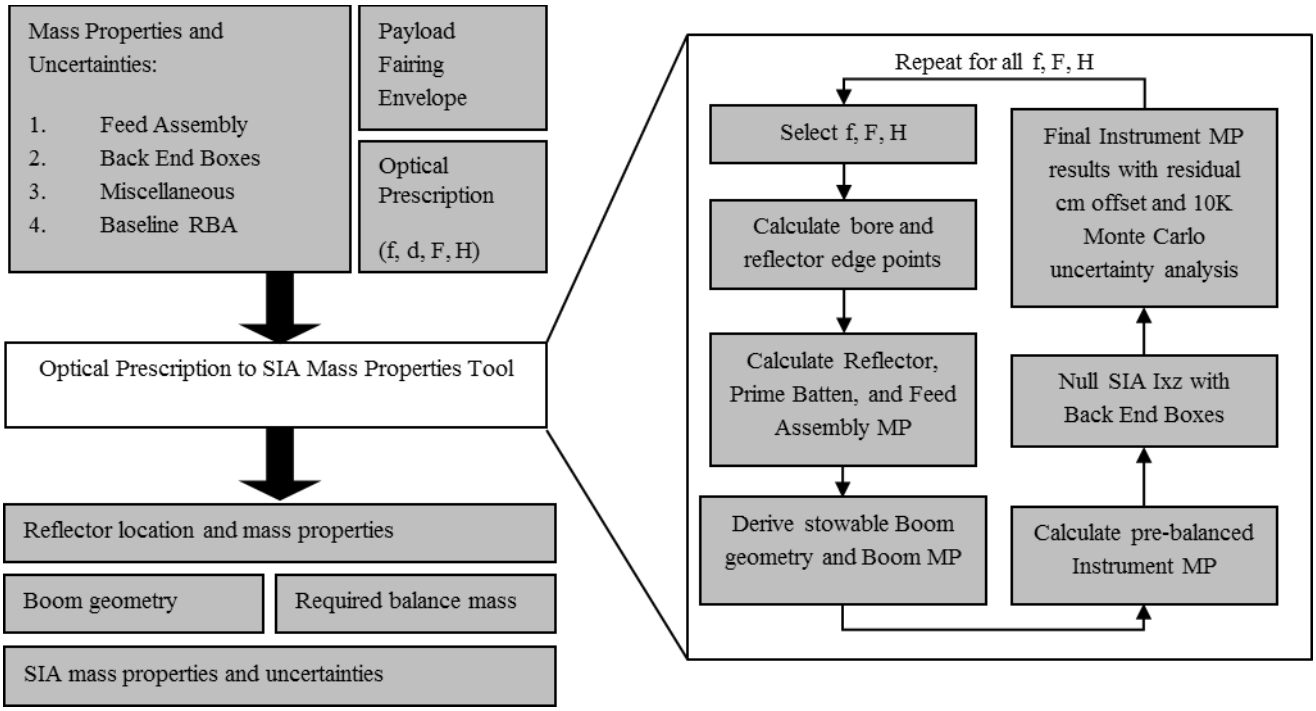

Figure 4 - RF prescription optimization algorithm.

properties requirements were drafted (Table 2), a limit on the magnitude of this torque was established.

III.RF Prescription Optimization

While the EPOI balancing approach was being formulated, a parallel effort to improve the balancability of the Spun Instrument was in progress. The RF prescription optimization campaign was intended to create a Spun Instrument that was statically and dynamically balanced in a nominal state, had a low sensitivity in the Ixz plane, had a low sensitivity to component mass and center of mass changes, and possessed a low Izz. For this study, the Iyz plane was ignored as it was largely symmetric. Software was developed to optimize the physical configuration of the system by searching through RF prescription space. As shown in Figure 4, the algorithm:

- Scanned the available RF focal points (fx, fz), focal lengths (F), and reflector edge offsets (H)
- Calculated the Reflector orientation, depth, and mass properties at each prescription
- Automatically generated a boom geometry (and boom mass properties) that both interfaced with the Reflector and stowed within the launch vehicle fairing
- Balanced the Spun Instrument using the Back End Electronics and balance mass (Figure 6)
- Performed a 10000 case Monte Carlo uncertainty analysis for each optical prescription configuration to determine its sensitivity to developmental changes

After completing this process, a viable prescription that reduced the Spun Instrument sensitivity to center of mass offset and product of inertia was identified.

A. RF Parameters

The SMAP RF Prescription was defined by a focal point (fx,fz), edge offset (H), focal

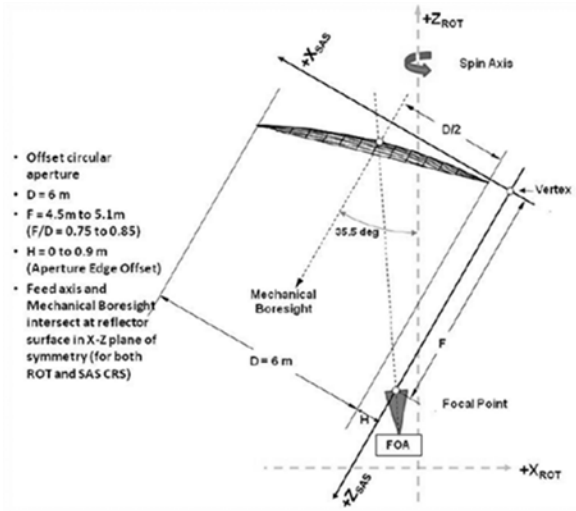

Figure 5 - Reflector geometry showing focal length, edge offset, focal point, and look angle.

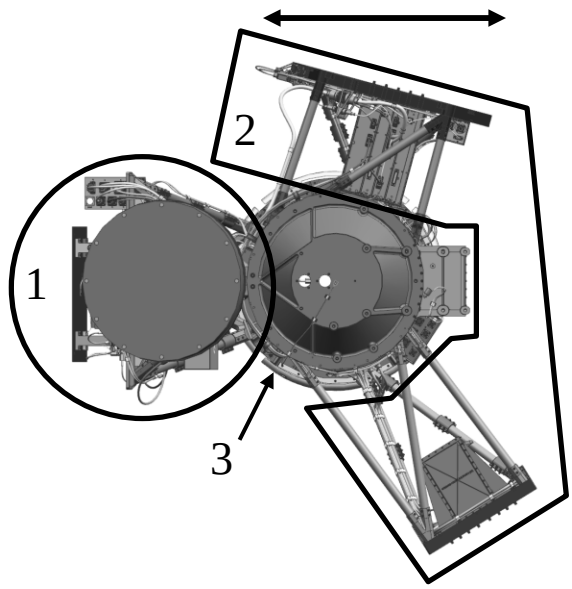

Figure 6 - Spun Instrument component groupings used in optimization. View is in the –Z direction. Subassemblies are the Integrated Feed Assembly (1), Back End Electronics (2), Miscellaneous (3), Reflector/Prime Batten (4) (Figure 2), and Boom Assembly (5) (Figure 2). Back End Electronics were permitted to move in the vehicle X direction to help null Spun Instrument Ixz.

length (F), and reflector diameter (d) (Figure 5).

For this study, symmetry about the XZ axis was assumed (fy = 0). F/d ratios of 0.7 to 0.9 and H values of 0 to 900 mm satisfied the radar and radiometer requirements of the

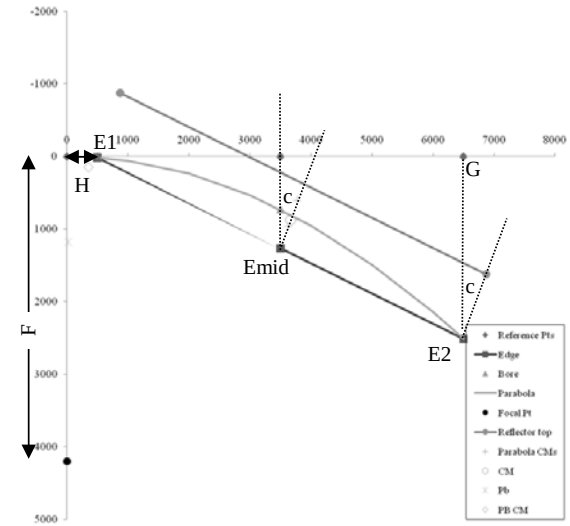

Figure 7 - Reflector points and rough Reflector structure outline in the parabolic mesh (SAS) frame.

mission. The look angle of the SMAP instrument was fixed at 35.5 deg. A 200 mm range of fx and a 200 mm range of fz values were examined. Since the mass properties depended on the physical (not electrical) properties of the reflector, a "structural edge offset" was generated. This brought the reflector to its physical diameter of 6.17 m, as opposed to its electrical aperture size of 6 m.

As shown in Figure 6, the SMAP Instrument was broken into five subassemblies for the study: Reflector/Prime Batten, Boom, Feed Assembly, Back End Boxes, and Miscellaneous (i.e. core structure, spin mechanism, etc.).

B. Parametric Reflector Design

The algorithm calculated the Reflector center of mass position, Reflector tilt, and the Feed Assembly tilt in the parabolic mesh (SAS) frame. This was accomplished by using the reflector edges (end points of the major axis) and center (reflector "boresight"). The Reflector surface was defined by

$$z_{sas} = \frac{(x_{sas})^2 + (y_{sas})^2}{4F} \tag{7}$$

where z_{sas} represents points on the reflector parabola and x_{sas} is equal to H, H+d/2, and H+d for E1, Emid, and E2 respectively (Figure 7). Y_{sas} was ignored due to symmetry. The depth of the Reflector was calculated by

$$c = 90 - \cos^{-1}\frac{\left(\overline{GE_2}^2 + \overline{E_1E_2}^2 - \overline{GE_1}^2\right)}{2\,\overline{GE_2}\,\overline{E_1E_2}} \tag{8}$$

$$\overline{AE_{mid}} = x_{sas,mid}\cos c \tag{9}$$

$$depth_{refl} = \overline{AE_{mid}}(1 + depthfactor) + ssd \tag{10}$$

where depthfactor was a fixed scaling factor for the depth of the rear mesh and ssd was the short spring distance (the fixed distance between the front and back mesh). The Reflector x center of mass (Cx) in the SAS frame was assumed to be on the centerline of the reflector ($\overline{\boldsymbol{AE_{mid}}}$). The Cz of the reflector in the SAS frame was measured as an offset from Emid and calculated as

$$Cz_{off} = \frac{j}{k}$$

$$j = \frac{2}{3}\overline{AE_{mid}}m_{lmesh} + \left(depth_{refl} - \frac{2}{3}\overline{AE_{mid}}depthfactor\right)\cdot m_{umesh} + \frac{1}{2}\,depth_{refl}m_{reflrem}$$

$$k = m_{lmesh} + m_{umesh} + m_{reflrem} \tag{11}$$

where m_{lmesh} was the mass of the lower mesh, m_{umesh} was the mass of the upper mesh, and $m_{reflrem}$ was the remaining reflector mass: truss elements, hinges, etc. Note that the difference in the mesh masses caused a shift in the Reflector center of mass.

The Prime Batten length was calculated using the Reflector depth plus a constant distance. This produced a location for the base of the Prime Batten, which served as the attachment point for the Boom tip and a starting point for the Prime Batten center of mass positioning (Figure 8). A constant linear offset was used for the Cx position.

The reflector edge points were transferred from the SAS frame to the Spacecraft frame by

$$x_{s/c} = x_{SAS}\cos(180 - angle_{look}) - z_{SAS}\sin(180 - angle_{look}) + x_{SASC} \tag{12}$$

and

$$z_{s/c} = x_{SAS}\sin(180 - angle_{look}) + z_{SAS}\cos(180 - angle_{look}) + z_{SASC} \tag{13}$$

where (x_{SAS}, z_{SAS}) were coordinates in the SAS frame, anglelook was the reflector look angle (35.5 deg), and (x_{SASC}, z_{SASC}) is the origin of the SAS coordinate system.

The reflector tilt in the Spacecraft frame (Figure 7) was calculated as

$$tilt_{refl} = \tan^{-1}\frac{E_{2z,S/C} - E_{1z,S/C}}{E_{2x,S/C} - E_{1x,S/C}} \tag{14}$$

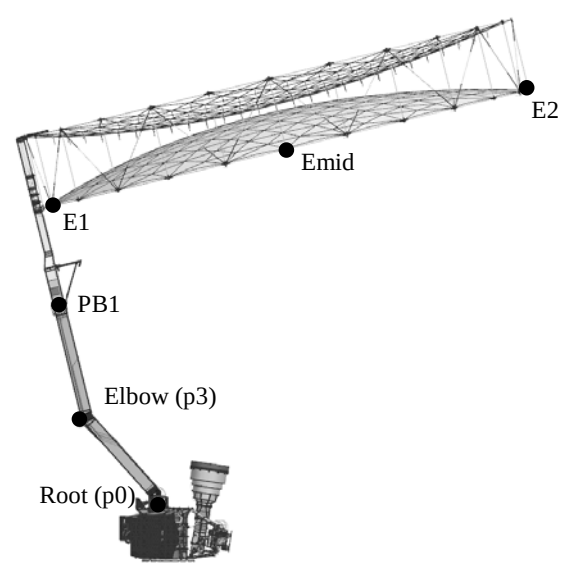

Figure 8 - Points for simplified RBA model. PB1 was the interface between the generated Reflector and Boom models.

The Reflector/Prime Batten center of mass was calculated by

$$C_x = \frac{\sum mx}{\sum m} \tag{15}$$

The Reflector/Prime Batten and the Feed Assembly Izz and Ixz were calculated by extrapolating the mass properties of the baseline design using

$$I_{zz,rot} = \frac{1}{2}\left(I_{xx,init} + I_{zz,init}\right) - \frac{1}{2}\left(I_{xx,init} - I_{zz,init}\right)\cos\left(2\left(tilt_{refl} - angle_{init}\right)\right) - I_{xz,init}\sin\left(\left(tilt_{refl} - angle_{init}\right)\right) \tag{16}$$

and

$$I_{xz,rot} = -\frac{1}{2}\left(I_{xx,init} - I_{zz,init}\right)\cdot \sin\left(2\left(tilt_{refl} - angle_{init}\right)\right) + I_{xz,init}\cos\left(2\left(tilt_{refl} - angle_{init}\right)\right) \tag{17}$$

were $I_{zz,rot}$ and $I_{xz,rot}$ were the new inertia parameters, $I_{xx,init}$, $I_{zz,init}$, and $I_{xz,init}$ were the initial inertias, and $angle_{init}$ was the initial angle.

C. Boom Design

As the Reflector/Prime Batten shifted and tilted through RF prescription space, the Boom geometry also changed. For a defined root (p0) and tip position (p6) (Figure 9), the boom geometry was

$$p_{x,des} = a_1\cos(t_1) + a_2\cos(t_1+t_2) + a_3\cos(t_1+t_2+t_3) + a_4\cos(t_1+t_2+t_3+t_4) + a_5\cos(t_1+t_2+t_3+t_4+t_5) + a_6\cos(t_1+t_2+t_3+t_4+t_5+t_6) + p_{ox} \tag{18}$$

and

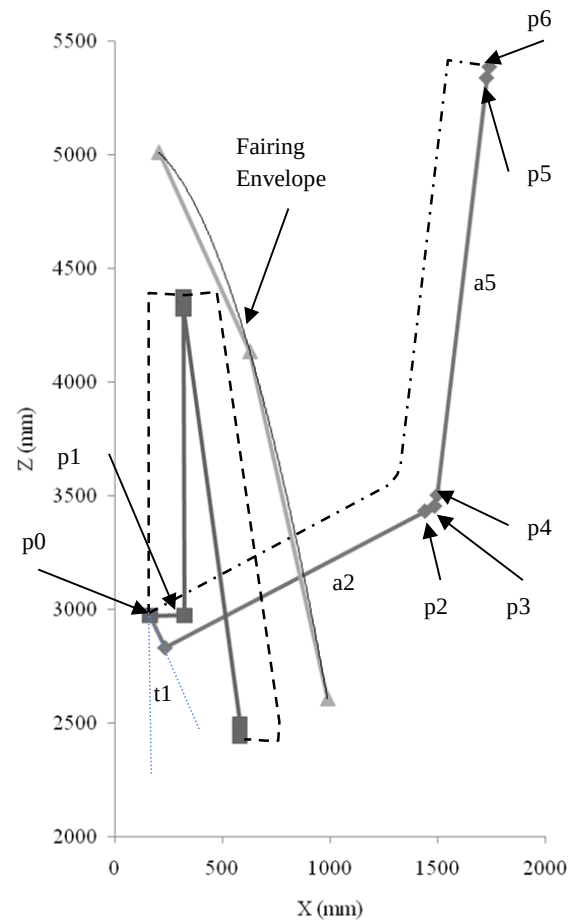

Figure 9 - Boom geometry. Note that small segments are short "kinks" in the boom. Segment length (a) and angle (t) labels follow as implied. Dotted lines show full Boom thickness.

$$p_{z,des} = a_1\sin(t_1) + a_2\sin(t_1+t_2) + a_3\sin(t_1+t_2+t_3) + a_4\sin(t_1+t_2+t_3+t_4) + a_5\sin(t_1+t_2+t_3+t_4+t_5) + a_6\sin(t_1+t_2+t_3+t_4+t_5+t_6) + p_{oz} \tag{19}$$

where $a_{1\text{-}6}$ are lengths of the boom segments, $t_{1\text{-}6}$ are the angles of each joint, and (p_{ox}, p_{oz}) is the root hinge position. The angle of the tip at the Prime Batten interface was

$$\varphi = t_1 + t_2 + t_3 + t_4 + t_5 + t_6 \tag{20}$$

For a viable geometry, the Boom must both reach the Prime Batten interface point and fit within the launch vehicle faring while mated to an appropriate stowed reflector

point. The faring envelope was simplified to the following parabola

$$z = -0.0028x^2 + 0.2283x + 5080.2 \qquad (21)$$

where x and z are in mm. These equations were solved simultaneously with the appropriate constraints on object positioning. As an approximation, the p3 (elbow joint) was placed on the parabola line described in Equation 21 (a constraint of the solver). P6 was placed on the desired Prime Batten interface location in the stowed and deployed RBA states (Figure 10).

A mass/length was applied to each boom segment, which accounted for the changing composite boom mass and cabling. This mass was applied at the midpoint of each Boom segment. Point masses were applied at the root, elbow, and tip to account for actuators and hinges. Rectangular prisms were assumed for the boom segments, and rotated inertia parameters (Izz and Ixz) were generated using Equation 16 and 17. The Boom center of mass was calculated using Equation 15. The Boom inertia was calculated by

$$I_{zz} = \sum I_{zz,i} + m_i\left((x_i - C_x)^2 + \left(y_i - C_y\right)^2\right) \qquad (22)$$

and

$$I_{xz} = \sum I_{xz,i} + m_i(x_i - C_x)(z_i - C_z) \qquad (23)$$

where y and Cy (y center of mass) are zero.

D. System Balancing and Uncertainty Calculation

Using the Reflector/Prime Batten, Boom, Feed Assembly, and Miscellaneous component mass properties, the initial unbalanced Spun Instrument was calculated. Equation 23 drove the Back End Box placement to an x station which resulted in a zero Ixz for the Spun Instrument. The resulting mass properties were then calculated to determine the center of mass offset and Izz.

Item	M (%)	Cx (mm)	Cz (mm)	Izz (%)	Ixz (%)
Reflector Prime Batten	-0 +10	± 15	± 15	-0 +10	± 10
Boom	-0 +15	± 15	± 15	± 15	± 15
Feed Asm	-0 +30	± 25	± 25	-15 +30	± 30
Back End Boxes	-0 +30	± 20	± 25	-15 +30	± 30
Misc.	-0 +30	± 25	± 25	-15 +30	± 30

Table 3 - Monte Carlo uncertainties.

After completing this calculation, it was possible to select a statically and dynamically balanced Spun Instrument configuration that required zero balance mass in a nominal condition. However, this result did not allude to the system stability through the course of development in and of itself. In order to determine the uncertainty in the as-built Back End Box position and long term balance mass use, the masses of the Reflector/Prime Batten, the Feed Assembly, and the Back End Boxes were adjusted. The system was rebalanced for each case. This yielded the range of Back End Box x positions required to maintain the dynamic balance of the Instrument using configuration flexibility only (no balance mass) through the course of the project.

A 10,000 case Monte Carlo run was computed for each RF prescription, varying m, Cx, Cz, component Izz, and component Ixz by the values shown in Table 3 over a uniform distribution. These calculations were run using a fully balanced Spun Instrument, and the system was not rebalanced afterwards. This represents uncertainties that would appear through the development of the

Observatory after fixing the Reflector F and H.

E. Results

The Cx for the Spun Instrument was plotted against F and H, shown in Figure 10. What followed was a minimum Cx, or "optimum F-H" line.

As F increased (Figure 11), there was a general increase in the Ixz contribution of the Boom and a general decrease in the Reflector/Prime Batten Ixz. The rest of the components remained relatively constant.

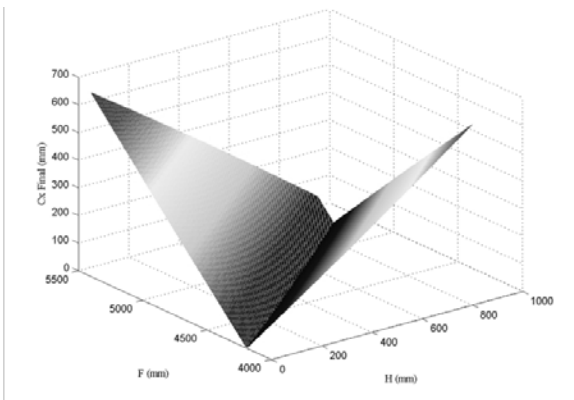

Figure 10 - Spun Instrument Cx vs. F and H for dynamically balanced configurations. Minimum Cx line represents statically and dynamically balanced Instrument configuration.

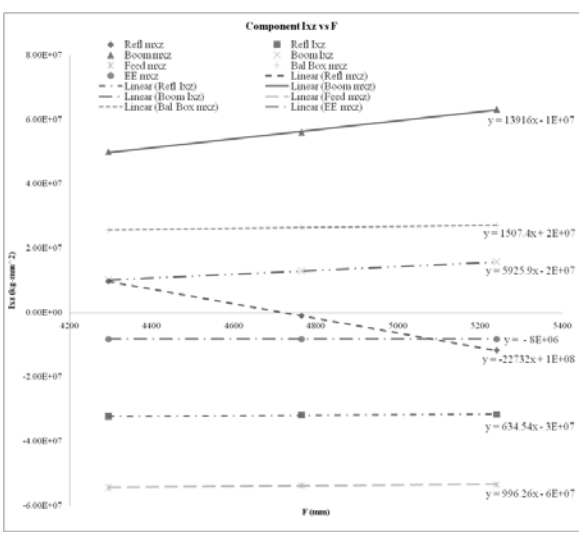

Figure 11 - Change in component Ixz contribution to system POI due to geometry and center of mass shift vs. F.

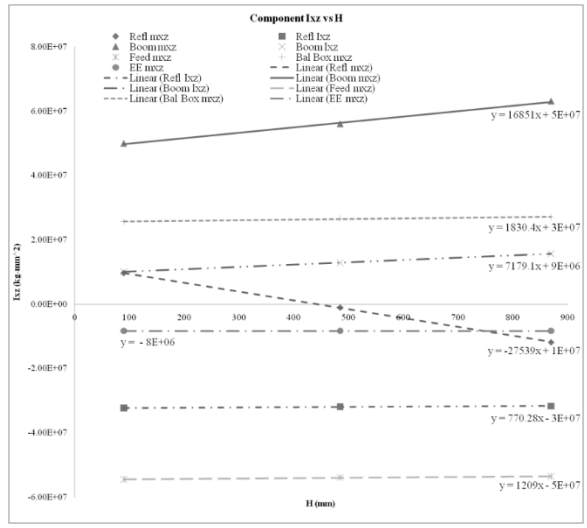

Figure 12 - Change in component Ixz contribution to system POI due to geometry and center of mass shift vs. H.

This same trend was seen for varying H (Figure 12). This natural "self-cancelation" effect along the optimum F-H line allowed for the appearance of statically and dynamically balanced configurations.

The 1% and 99% Monte Carlo Ixz uncertainties were plotted against F and H, shown in Figure 13. As the focal length F decreased, the Reflector/Prime Batten and Boom "mxz" term of Equation 23 decreased. This effectively reduced the Spun Instrument Ixz uncertainty due to component center of mass uncertainty. The additive effect of component Ixz (the first term of Equation 23) could not be reduced in sensitivity through geometric modifications to the Instrument configuration. Understanding and controlling this parameter formed a large part of the SMAP mass properties effort. Fortunately, Izz and Cx offset did not increase dramatically (<5%) over the range of F and H.

An RF prescription of f = (-515.4, 2908.2) mm, F = 4200 mm, and H = 10 mm (structural edge offset) was selected as a baseline. When the RF prescription was corrected from the structural offset, the

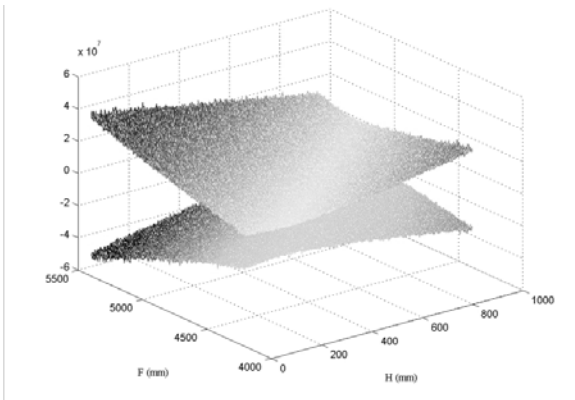

Figure 13 - 1% and 99% Monte Carlo SIA Ixz (kg-mm^2). Minimum Ixz uncertainty exists at low F, H.

electrical edge offset H became 104.1 mm. For system dynamic balancing, a Back End Box x position range of 123 mm was enough to satisfy all potential Spun Instrument Ixz values given JPL design phase mass uncertainties.

A Monte Carlo study was conducted by varying the initial component mass properties inputs and recalculating the optimum F-H line for each new set (Figure 14). The result was a most probable F-H line for uniformly distributed design phase uncertainties. This line was plotted against the current best estimate (CBE) F-H line from the baseline Instrument, shown in Figure 15. It can be seen that component mass properties uncertainties do not drive the Optimum F-H

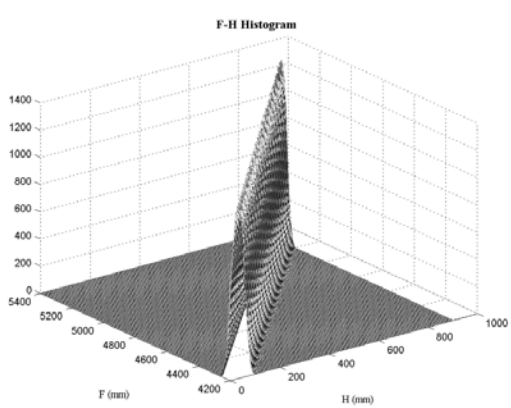

Figure 14 - Probabilistic distribution of optimum F-H lines for design phase uncertainty inputs.

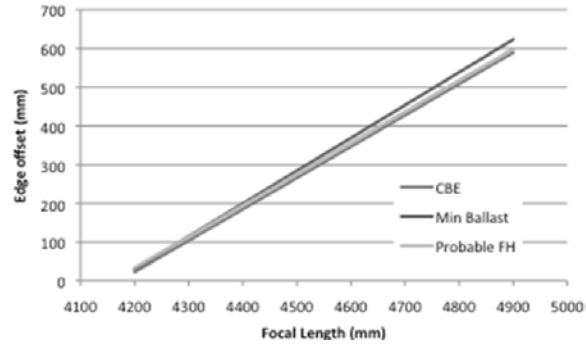

Figure 15 - Probable F-H line and current best estimate (CBE) F-H line for baseline Instrument.

line from the CBE F-H line. The slope of this minimum balance mass line is described by Equation 24, where subscript 1 represents the mass properties of the Spun Platform Assembly (SPA) and subscript 2 represents the mass properties of the Reflector/Boom Assembly (RBA).

$$\frac{\delta H}{\delta F} = -\frac{n}{o}$$

$$n = m_1\left(x_1\frac{dz_1}{dF} + z_1\frac{dx_1}{dF}\right) + \frac{dI_{xz}^1}{dF} + m_2\left(x_2\frac{dz_2}{dF} + z_2\frac{dx_2}{dF}\right) + x_2 z_2\frac{dm_2}{dF} + \frac{d_{xz}^2}{dF}$$

$$o = m_1\left(x_1\frac{dz_1}{dH} + z_1\frac{dx_1}{dH}\right) + \frac{dI_{xz}^1}{dH} + m_2\left(x_2\frac{dz_2}{dH} + z_2\frac{dx_2}{dH}\right) + x_2 z_2\frac{dm_2}{dH} + \frac{d_{xz}^2}{dH} \quad (24)$$

The final selection of the SMAP RF prescription was made in the presence of large uncertainties. After F and H were selected, the Feed Assembly and Reflector were fixed in space, restricting the ability to adjust the system mass properties at a large scale. One adjustment lever that remained open for a short time, however, was the Boom geometry. While the Reflector was defined by a strict F and H, there were many Boom designs (with many Ixz's) that could accommodate the selected RF Prescription. While the final Boom design was selected shortly after the RF prescription, the delay allowed for some compensation for design changes in the intermittent months. The same

tools used for the RF prescription optimization algorithm were used for the Boom geometry optimization.

IV. Configuration Flexibility

While the Reflector F and h were locked down early in the project, the final location of the two electronics assemblies was left open until six months before CDR. This was used as a way to counter the EPOI of the Spun Instrument while reducing the need for balance mass. The radiator and truss design implemented on SMAP facilitated this late-game configuration flexibility. After examining the configuration, the RDE/RBE Assembly was found to be "blocked in" by various keep-out zones and structural envelopes (Figure 16). This left the ICE Assembly as a potential adjustment mechanism. Three degrees of freedom were available: radial position, z-station, and angular position around the SPA. A set of (x,y,z) coordinates for this assembly center of mass were explored, and a contour graph was generated for the 99.73 percentile balance mass required for each ICE Assembly position. A final ICE position was selected based the predicted minimum balance mass location.

F. Balance Mass Strategy

At the beginning of the mission, it was envisioned that balance mass would be applied on the Spun Platform Assembly (SPA) to correct static and dynamic imbalances. An allocation of 10 kg was provided by the project to correct for both. It was quickly determined that this was not sufficient to balance the system. Fortunately, the large size of the Reflector Boom Assembly permited mass to be placed far from the spin axis of the vehicle. By utilizing these locations, it was possible to realize significant reductions in balance mass amount while increasing balancing capability. That said, the same thing

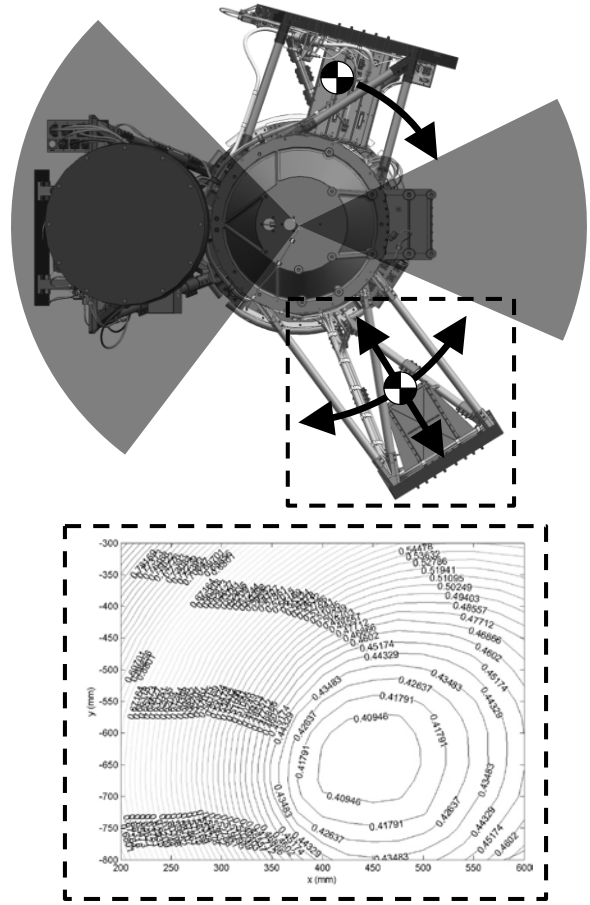

Figure 16 - Position flexibility for each Back End Electronics assembly. Grey sectors are keep out zones. Contour plot shows balance mass required for a given assembly position at a given Z-station.

that made these locations powerful mass properties levers also made them extremely sensitive. Much care was exercised in the selection and application of the final balance mass amount.

23 locations were available on the valley nodes of the Reflector (Figure 2). Each of these locations could support a maximum of 0.1 kg of tungsten balance mass, while the Reflector rim could hold 0.5 kg total. JPL controlled the location and application of this mass through the course of the project and used it to balance the spinning system. An additional balance mass location was available on the Prime Batten of the Reflector that could support up to 0.8 kg of balance mass. For the majority of the project, this was controlled by Astro Aerospace and used to reduce the flux of their Reflector mass

Figure 17 - Reflector rim balance mass. Stacks were used to fine tune balance mass amount.

properties though the course of development.

JPL optimized both the Reflector rim and Prime Batten balance masses together for the final balancing operations. After all testing was completed and the final analysis was run, 0.090 kg of balance mass was applied to the Reflector, minimizing the EPOI in both axes. The Prime Batten balance mass (0.8 kg) was not utilized. The predicted EPOI after balancing was:

- eIxz: 0.018 ± 0.9 kg-m^2
- eIyz: 0.136 ± 0.7 kg-m^2

It should be noted that unlike the Spun Instrument, the delivered Observatory was not precision balanced to meet launch vehicle mass properties requirements. Instead, two 10 kg brass masses were used to shift the stowed Observatory mass properties towards the centerline of the vehicle en masse. This increased the control margin of the vehicle.

V.Elimination of Balancing Mechanism

Two On-Orbit Balancing Mechanisms (OBMs) were originally included on the SMAP Spun Instrument for the purpose of reducing residual EPOI after launch. 4 kg out of the 20 kg mechanism mass was movable. This could have adjusted the system EPOI by ±1.9 kg-m^2. A number of placement options were examined to maximize EPOI adjustability and minimize impact on the Spun Instrument structure. In the end, the relatively low impact of the OBMs on the Spun Instrument EPOI and their contribution to the Izz of the Spun Instrument led to their eventual descope. It was believed that a combination of smart pointing error budgeting and rigorous mass properties analysis, tracking, and test would prove to be sufficient to control imbalances.

VI.Observatory Mass Properties Tracking and Analysis

The mass properties for the Instrument and Observatory were managed continuiously by the JPL mass properties engineer in conjunction with the JPL project resource engineer (holder of Mass Equipment List). The RBA mass properties were managed by Astro Aerospace with guidance from the JPL mass properties engineer. A system level scrub and balancing effort was performed quarterly.

A standard data format was used across all tools. Mass properties were tracked using a Microsoft Access database. Calculation and balancing operations were conducted using custom Matlab software developed during this project with Excel as an input sheet. The base calculation suite consisted of a nominal and uncertainty mass properties calculation script along side an Instrument and Observatory balancing script. Both relied on Monte Carlo analysis, as opposed to RSS/Error Propagation Equation uncertainty calculation methods. This was done to leverage unequally distributed uncertainty ranges for components, resulting in a net reduction in the overall uncertainty range and

balance mass allocation required. On hardware deliverly, a digital Excel-based form was used to collect mass properties information for each component.

VII.Mass Properties Knowledge

A series of component, subassembly, and assembly level mass properties testing was implemented to verify and improve the analytical mass properties models developed through the course of the project. Simplified testing of subassemblies was employed to reduce the complexity and hardware risk of a full assembly mass properties measurement. Tests were selected for their ability to improve knowledge of the EPOI parameters:

- Spun: mass, Cx, Cy, Cz, Ixz, Iyz
- Despun: mass, Cz

A. Spacecraft Panel Testing

Three of the four integrated Spacecraft Panels were measured on a Space Electronics KGR-500 to quantify their center of mass in two axes and moment of inertia in one. The panels integrated vertically on the Spacecraft, so it was straightforward to measure their contribution to the Despun Cz by testing horizontally. An adapter was created to attach a pre-existing panel handling fixture to the KGR-500. A pin and slot was used to ensure that the handling fixture could be reattached in the same position for a tare measurement after the panel was removed.

When the panel state was known accurately before a test, the measurement correlation to the model was extremely close and within pre-test uncertainties. Given the large inertia values for these panels, the KGR-500 had to be manualy damped by hand prior to the machine conducting the measurement. This was accomplished by lightly gripping the rotating shaft immediately after the machine reached its measurement position.

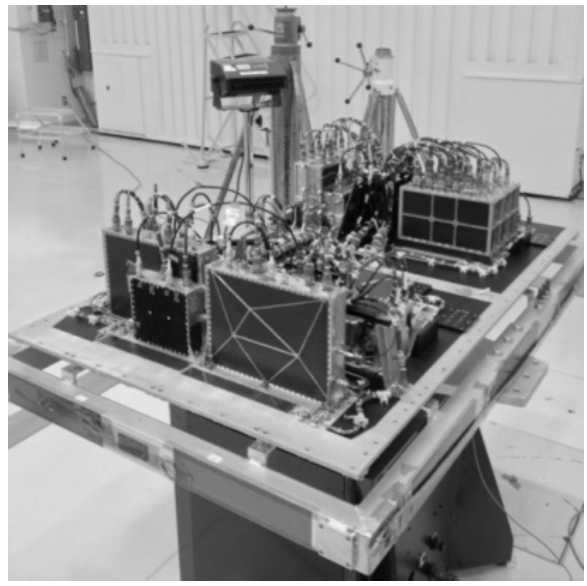

Figure 18 - Center of mass and moment of inertia measurement of an integrated Spacecraft panel. The mass properties testing was scheduled to capture as much integrated harness as possible.

B. Spun Platform Assembly (SPA)

The SPA represented the largest spinning mass that could undergo a direct, dynamic product of inertia measurement. For testing, it was mounted to a Space Electronics POI-12000 table using a custom fixture. The SPA was mounted offset from its spin axis in order to bring the center of mass of the assembly closer to the spin axis of the machine. This reduced the uncertainty of the measurement. Counterweights were added to the test fixture to bring its center of mass closer to the table spin axis. A laser tracker was used to measure the location of the POI-12000 and INSR coordinate systems to within ±75 microns translational and ±10 millidegrees rotational of true position.

One of the largest areas of uncertainty for this test was the effect of windage. Most JPL product of inertia measurements are conducted on Mars-bound aeroshell-enclosed spacecraft. This largely eliminates lift and drag torques on the vehicle (barring the effect of appendages). It was not known whether the asymmetric SPA (Figure 19)

would cause problems at the 30 RPM test spin rate. Six possible effects were identified:

- Inability to reach measurement speed
- Inability to maintain measurement speed
- Asymmetric drag torques
- Lift
- Aerodynamic Deflection
- Turbulence or Aerodynamic Vibration

Rough analyses were conducted on simplified versions of the various SPA appendages to gage if they would create aerodynamic errors during the measurement. The first five sources could be mitigated by spinning the SPA both clockwise and counterclockwise, then averaging the results. Turbulence was not quantifiable in this pretest analysis, however it was agreed that if these effects were present, they would increase their random contributions to the

Figure 19 - SPA on POI-12000 during measurement

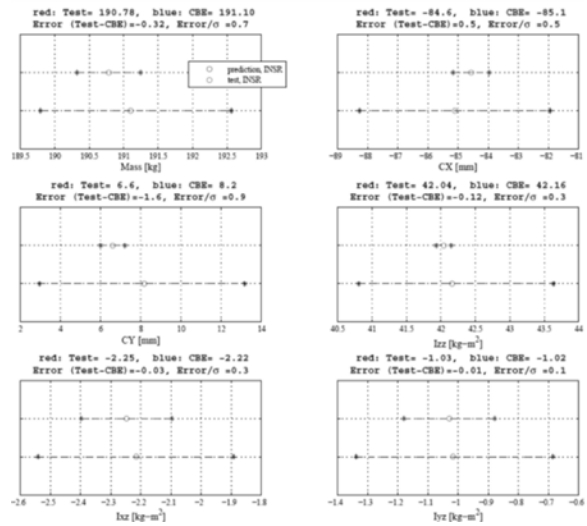

Figure 20 - Spun Platform Assembly predictions (bottom line) and results (top line). All but one prediction fell within the uncertainty bounds of the measurement.

measurement error as the test speed was increased. A number of spins at 45 RPM were planned to verify that turbulence was present if the 30 RPM measurements were excessively noisy. In the event significant errors were induced, materials for an aerodynamic shroud were procured. This shroud was non-spinning, and designed to closely encapsulate the volume of air surrounding the SPA. As the SPA spun, the air would eventually reach the same rotational speed, reducing turbulent effects.

As shown in Figure 20, the measurement of the SPA fell extremely close to the predicted mass properties. All measurements fell within the predicted uncertainty bounds, and all but one pre-test prediction fell within the uncertainty bounds of the measurement. The center of mass was predicted within 0.5 mm in the Cx axis, and 1.5 mm in the Cy. All inertias were within 0.3 sigma of their predictions. These results demonstrate the extremely good correlation between the analytical mass properties model and the as-built flight hardware. Few, if any signs of turbulence or aerodynamic vibration were observed during the test. The 45 RPM

measurements were not conducted, and the shroud was not used.

C. Boom and Prime Batten Testing

While it was not possible to measure the mass properties of the Reflector Boom Assembly in its flight configuration, accurate measurements of the large structural elements were relatively straightforward. The Prime Batten was tested twice at Astro Aerospace's Goleta facility on JPL's KGR-500 machine. The first measurement occurred on the base carbon fiber structure (the Bonded Prime Batten), while the second was performed on the fully integrated Prime Batten. An 80/20 fixture was constructed by the vendor to restrain the test article and orient all loose harnesses in their flight orientation. Buy measuring in two rotational orientations (0 and 90 degrees), all three center of mass coordinates and two moments of inertia values were obtained.

The Boom was tested at JPL on a KGR-500. This test was very similar to the Prime Batten in that a fixture was used to position the integrated Boom in two orientations. A large amount of shimming was required to ensure that the Boom was sitting in a free state when mounted. Additionally, a significant amount of balance mass was required to reduce the tare moment present on the KGR-500 due to large test fixture center of mass offsets. Even with this balance mass, there was a significant moment on the machine that reduced the accuracy of the measurement.

On both measurements, the KGR-500 had to be damped by hand to reduce the oscillations caused by the large moment of inertia of the test assembly.

D. Reflector Testing

Of all the components on the RBA, the Reflector mass properties were the most critical to understand. The deployed Reflector test was tentatively planned since the beginning of the project; however it was unclear if accurate results would be possible. Even if successful, it was not clear whether the uncertainty of measured results would be definitive enough to validate the Reflector mass properties models. In the end, a test was performed with predicted test uncertainties larger than analytically modeled uncertainties. It was decided that if the test results agreed with the model, the model would be used. If the test results disagreed with the model results, the test results would be used to diagnose errors in the model.

Given the 6 m diameter of the Reflector, it was not possible to use the KGR-500 for this test. Instead, a three scale center of mass measurement was selected. The test was originally planned using three tensile load cells to perform two, 2-axis planar center of mass measurements. The third measurement, to be accomplished by tilting the Reflector (elevating one point), was descoped due to the added complexity and hardware risk. A lack of accurate tensile load cells forced a switch to compressive tabletop scales. Ball/plane interfaces were used on each scale

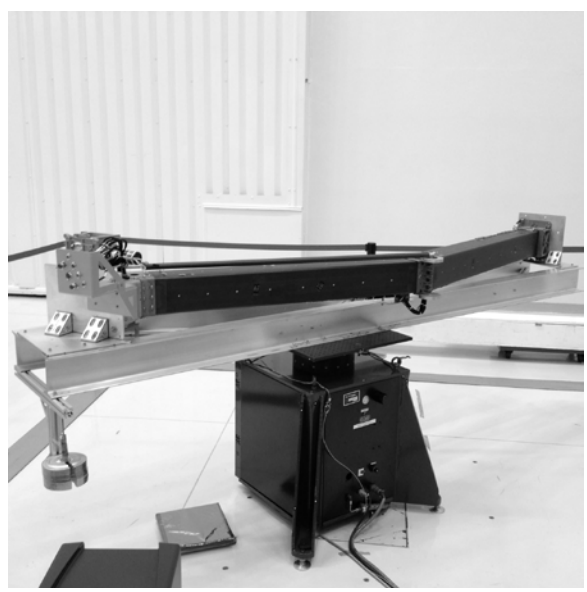

Figure 21 - Boom on KGR-500 during measurement. Note balance mass used on fixture.

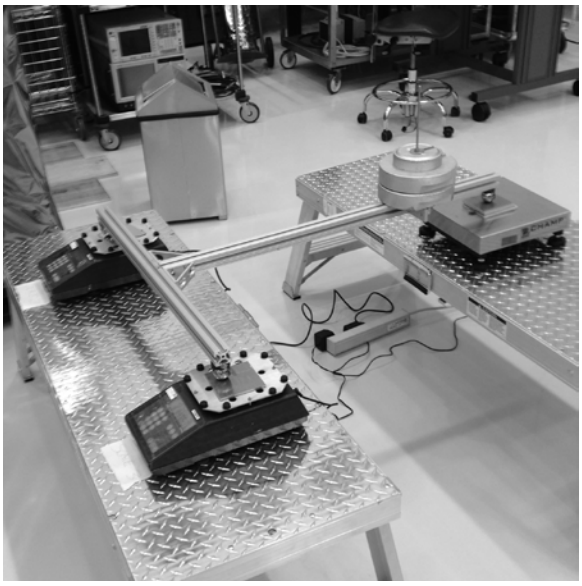

Figure 22 - Reflector center of mass pathfinder measurement.

to reduce the probability of a side load or imparted moment.

A detailed error analysis was performed by JPL to determine if a three scale measurement would be feasible. Error sources included the following:

- Scale measurement uncertainty after calibration
- Measurement error due to side load
- Remaining scale tilt after leveling
- Lean error due to different deflections of scales under load
- Hysteresis under load
- Drift over time
- Vibration due to foot traffic
- Windage due to drafts
- Position uncertainty (metrology)
- Reflector deflection during test

The test error budget estimated a total potential error between 6 and 13 mm (RSS and sum of the sources, respectively).

To achieve this accuracy, a number of steps were taken while conducting the test. Each of the scales was calibrated in situ hours before the test was conducted, and leveled to better than ±0.3 degrees. All weighing pans were replaced with precision MIC6 plates to encourage slipping, thus reducing scale side loads. A side load checkout was performed on each scale, and it was found that each could tolerate a force well above the coefficient of static friction of the ball/plane interface without significant added error. An Astro Aerospace FEA model of the Reflector was used to determine that its deflection due to gravity would have almost no effect on the load at each scale location.

An Ohaus CQ25-R11 was used at the Prime Batten support point while two Setra 12000C scales were used near the Reflector tip. The use of two scale sensitivities allowed the test setup to both support the full weight of the Reflector and get additional load measurement accuracy near the Reflector tip. Adapters were developed to allow spherical mounted retro-reflector (SMR) nests to be mounted to three locations on the Reflector rim. Each 1.5 inch SMR acted as both a metrology point and a ball interface to the scale. Prior to running the official measurement, a pathfinder test was run on an 80/20 surrogate of equal mass. The surrogate center of mass was verified for accuracy by a KGR-500 measurement.

The measurements performed were more consistent than expected, and led to uncovering several undiagnosed errors in the Reflector mass properties FEA model, shown by the center of mass offset in Figure 24.

VIII.In Flight Performance

SMAP successfully launched from Vandenberg Air Force Base on January 31, 2015. After 34 days in orbit, the Instrument was spun up to its 14.6 RPM operational speed. On-orbit data from the SMAP inertial measurement unit (IMU) revealed that the in-flight wobble was approximately 50

millidegrees, 25% of the 200 millidegree requirement (Figure 25). This translated to an approximate EPOI of

- eIxz: 0.73 kg-m^2
- eIyz: 0.58 kg-m^2

These values sit within the bounds of the pre-flight predictions:

- eIxz: 0.018 ± 0.9 kg-m^2
- eIyz: 0.136 ± 0.7 kg-m^2

While the EPOI appeared to match, the Izz of the Instrument came in more than 3-sigma below what was expected. Though an exact cause is not known, 0.239 kg of missing mass around the Reflector rim could produce the noted effect.

IX.Conclusion

The success of this effort was due to a methodical approach to identify and buy down uncertainty through configuration flexibility, detailed tracking, and high accuracy subassembly testing. When examining the system as it stood on delivery, it was clear that the initial static and dynamic balance requirements would not have been possible to meet. The choice to move to an Effective Product of Inertia architecture was critical in the success of this mission. Additionally, the low focal length selected significantly reduced the sensitivity of the system to late-game changes in the Reflector Boom Assembly. The three tiered approach of RF-Prescription, Back End Box location, and Reflector Balance Mass provided resiliency to mid- and late-project changes.

At a higher level, the successful implementation of an asymmetric spinning deployable Reflector on SMAP opens the door for a variety of large aperture radar instruments not previously thought possible.

Figure 23 - Reflector center of mass measurement scale setup. Note SMR used as a both a metrology target and ball interface to the scale.

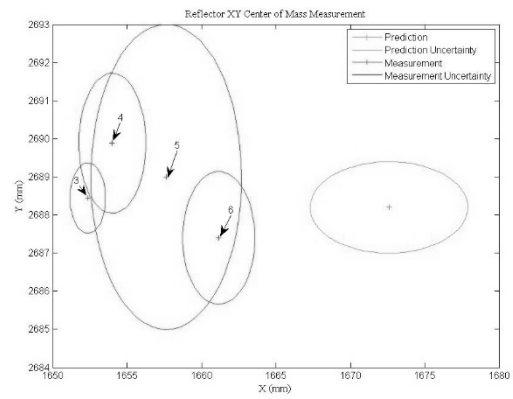

Figure 24 - Reflector center of mass measurement test results. Measured values are clustered on the left. The offset test prediction on the right highlights the modeling error discovered in the test.

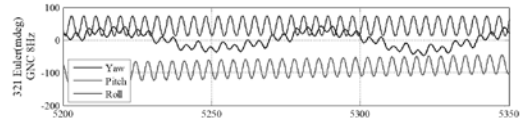

Figure 25 - SMAP flight IMU data. The resulting wobble of approximately 50 mdeg is shown as the high frequency oscillation on the top and bottom trace.

The lessons learned on SMAP should prove helpful in developing these future missions.

SMAP is managed for NASA's Science Mission Directorate, Washington, by NASA's Jet Propulsion Laboratory, Pasadena, California.

Acknowledgments

The research was carried out at the Jet Propulsion Laboratory, California Institute of Technology, under a contract with the National Aeronautics and Space Administration.

The authors would like to thank the following individuals for their help during the course of this effort: Douglas Adams, Oscar Alvarez-Salazar, Robert Burke, Dan Eldred, Sasha Eremenko, Keith Fields, Pam Hoffman, Jason Kastner, Steve Kuehn, Ryan Meschewski, Mehran Mobrem, Reza Nayeri, Yuki Salinas, Sarah Sherman, Lisa Sievers, Chris Spier, Robert Stephenson, Mark Thomson, and Pete Waydo.

Bibliography

Alvarez-Salazar, O. S., et. al. "Pointing Architecture of SMAP's Large Spinning Antenna." Guidance, Navigation, and Control Conference. Boston, MA, August 2013.

Boynton, R and Wiener, K. "Design of Fixtures for Mass Properties Measurement." 54th Annual Conference of the Society of Allied Weight Engineers, San Diego, CA, May 1995. Society of Allied Weight Engineers Technical Paper Number 2190.

Boynton, R. "Fundamentals of Dynamic Balancing." 42nd Annual International Conference on Mass Properties Engineering, Anaheim, CA, May 1983. Society of Allied Weight Engineers Technical Paper Number 1504.

Boynton, R. "Mass Properties Measurement Handbook." Annual Conference of the Society of Allied Weight Engineers, Wichita, Kansas, May 1998. Society of Allied Weight Engineers Technical Paper Number 2444.

Boynton, R. "The Moment of Inertia of Fluids." 58th Annual Conference of the Society of Allied Weight Engineers, San Jose, CA, May 1999. Society of Allied Weight Engineers Technical Paper Number 2459.

Boynton, R. "The Moment of Inertia of Fluids -- Part 2." 59th Annual Conference of the Society of Allied Weight Engineers, St. Louis, MO, June 2000. Society of Allied Weight Engineers Technical Paper Number 3006.

Boynton, R. ""Standard" SAWE Mass Properties Calculation Software and Algorithms." 60th Annual Conference of the Society of Allied Weight Engineers, Arlington, TX, May 2001. Society of Allied Weight Engineers Technical Paper Number 3156.

Brayshaw, J. "Error Analysis of System Mass Properties." 43rd Annual Conference of Society of Allied Weight Engineers, Inc., Atlanta, GA, May 1984. Society of Allied Weight Engineers Technical Paper Number 1610.

Farr, R. G. "Ground Attitude Weighing of the YAH-64." 40th Annual Conference of the Society of Allied Weight Engineers, Inc., Dayton, OH, May 1981. Society of Allied Weight Engineers Technical Paper Number 1446.

Harvey, T. J. "Moments of Inertia of Liquids in Cylindrical Tanks." 17th National

Conference of the Society of Allied Weight Engineers, New York, NY, May 1958. Society of Allied Weight Engineers Technical Paper Number 184.

Jones, D. L. "Aerodynamic Effects on Spacecraft Dynamic Balance." 36th Annual International Conference of the Society of Allied Weight Engineers, Inc., San Diego, CA, May 1977. Society of Allied Weight Engineers Technical Paper Number 1166.

Marshner, R. L. "Aerodynamic Effects in Mass Properties Determination." 42nd Annual International Conference on Mass Properties Engineering, Anaheim, CA, May 1983. Society of Allied Weight Engineers Technical Paper Number 1506.

Mertzger, W. W. "Elimination of Aerodynamic Effects During Spin Balance of Spacecraft." 38th Annual Conference of the Society of Allied Weight Engineers, Inc., New York, NY, May 1979. Society of Allied Weight Engineers Technical Paper Number 1277.

Mobrem, M. et. al. "Design and Performance of Astromesh Reflector Onboard Soil Moisture Active Passive Spacecraft". IEEE Aerospace Conference, Big Sky, MT, March 2012.

Montgomery, J. A. and Haynes, R. W. "A Novel Approach to the Dynamic Balancing of Spun/De-Spun Spacecraft." Proceedings of the 21st Aerospace Testing Seminar. Journal of the IEST, V. 48, No. 1. Pg 12-20. 2005.

Nakai, J. H. and Tsai, W. "Center of Mass Uncertainty Coordinate Transformation." 71st Annual Conference of the Society of Allied Weight Engineers, Inc., Bavaria, Germany, May 2012. Society of Allied Weight Engineers Technical Paper Number 3570.

National Aeronautics and Space Administration. Jet Propulsion Laboratory. California Institute of Technology. "A Highly Accurate Method for the Determination of Mass and Center of Mass of a Spacecraft." JPL Technical Publication 78-2. Chow, E. Y., Trubert, M. R., and Egwuatu, A. April 15, 1978.

Slimko, E., French, R., and Riggs, B. "SMAP Instrument Mechanical System Engineering." IEEE Aerospace Conference. Big Sky, MT, March 2013.

Smith, C. H. "On-Orbit Balancing of a Large Flexible Spinning Antenna." (Masters of Science Dissertation). Massachusetts Institute of Technology. June 1986

Strom, G. J. "Matrix Methods for Mass Properties." 49th Annual Conference of the Society of Allied Weight Engineers, Inc., Mesa, AZ, May 1990. Society of Allied Weight Engineers Technical Paper Number 1946.

Tong, M. M., Smith, C. H., and Mak, P.H. "On-Orbit Balancing of a Spinning Antenna." AAS 87-480. Pg 895-914.

Biographies

Morgan Hendry completed his Bachelor's degree in Aerospace Engineering (Astronautics) and his Masters in Astronautics from the University of Southern California in 2005 and 2006, respectively. While there, he focused on robotics and autonomy, working at JPL and USC's Information Sciences Institute. In 2007, he began working full time at JPL on the Mars Science Laboratory Chassis Team as a

mechanical engineer. In 2009, he began work as the project mass properties engineer for the Soil Moisture Active Passive mission. After a successful launch and spin-up in early-2015, Morgan transitioned to developing reverse planetary protection technology to support future Mars Sample Return missions.

Eric Slimko received his PhD from the California Institute of Technology in Computation and Neural Systems in 2006 and his Bachelor's degree in Aerospace Engineering from the University of Michigan in 1994. He has been working at NASA's Jet Propulsion Laboratory since 1990 on a wide range of flight projects and technology programs relevant to entry systems. He was the Instrument Mechanical System Engineer for the Soil Moisture Active & Passive Mission.